Contactless and Short-Range Vital Signs Detection with Doppler Radar Millimeter-Wave (76 - 81 GHz) Sensing Firmware

[1,✉]Pi-Yun Chen, [1]Hsu-Yung Lin, [1]Zi-Heng Zhong, [1]Neng-Sheng Pai, [2]Chien-Ming Li, and [1,✉]Chia-Hung Lin

[1]Department of Electrical Engineering, National Chin-Yi University of Technology, Taichung City, 41170, Taiwan.
E-mail: ✉chenby@ncut.edu.tw, lin1620099471@gmail.com, ximen0806449@gmail.com, pai@ncut.edu.tw, ✉eechl53@gmail.com
[2]Chien-Ming Li is with the Division of Infectious Diseases, Department of Medicine of Chi Mei Medical Center, Tainan City, 710, Taiwan. **E-mail: 235813cmli@gmail.com.**
✉Corresponding Authors: Pi-Yun Chen (chenby@ncut.edu.tw), Chia-Hung Lin (eechl53@gmail.com)

***Abstract*:** Vital signs such as heart rate (HR) and respiration rate (RR) are essential physiological parameters used to assess human health and bodily functions. These can be measured via methods that either require or do not require direct contact. A non-contact Doppler radar millimeter (mm)-wave sensing firmware utilizes a 76–81 GHz (W-band) electromagnetic wave over a short-range path to the human body. It then processes the reflected electromagnetic wave to filter and extract human heartbeat and breathing rhythm signals. The short-range sensor system proposed herein eliminates the need for electrodes, electric patches, photoelectric sensors, and conductive wires, as well as the requirement for direct contact with the human body when measuring physiological signals. The W-band Doppler mm-wave sensing firmware, paired with frequency-modulated continuous wave radar, enables continuous monitoring of HR and RR. Short-wavelength mm-waves are employed in short-range detection to deliver highly precise measurements of physiological signals with minimal noise interference. Consequently, experimental tests were conducted in a laboratory setting to measure the heartbeats and breathing rhythm signals of healthy young men. Their HR and RR were estimated through frequency- and time-domain analyses. The experimental results confirm the feasibility of the proposed mm-wave radar for continuous human vital sign detection.

***Indexing Term*:** Heart Rate, Respiration Rate, Doppler Radar Millimeter (mm)-Wave, Frequency Modulated Continuous Wave, Vital Signs Detection.

1. Introduction

Assessing the functionality and condition of a heart can provide valuable information pertinent to the early detection of human emotional states, heart diseases, and cardiovascular-related conditions. Traditional heart rate (HR) and cardiac activity monitoring can be achieved through electrocardiography (ECG). This method uses three leads (leads I, II, and III) to measure electrical activity signals from the atria to the ventricles in the heart. An ECG reading exhibits a waveform, inclusive of the P wave, QRS complex wave, and T wave, and can be used to identify arrhythmia, heart conduction disorders, coronary ischemia, myocardial infarction, and atrial fibrillation. Regular contraction and relaxation activities in the atria and ventricles drive blood flow from the heart through the circulatory systems, including pulmonary and systemic circulation. Each heartbeat triggers a blood pressure wave passing through the blood vessels, causing regular pulsation as they contract and expand. Thus, Photoplethysmography (PPG) can be used to detect physiological parameters such as oxygen saturation (SPO_2), HR variability (HRV), and respiration rate (RR) [01–03].

ECG employs contact sensors that must be positioned on the human body, including the upper and lower limbs and chest. Electric patches or electrodes are attached to the skin to facilitate up to 12-lead measurements between any two attachments, enabling continuous monitoring of the heart's electrical activities. However, the quality of ECG measurements can be impacted by the setting environment and the dynamic state of the body, as subject movement may be restricted. PPG can operate in two modes: transmissive or reflective [02-03], using a photoemitter or photodetector. Photoemitters can measure visible green light (510 nm), visible red light (659 nm), or near-infrared (IR) light (800–940 nm). Photodetectors can observe changes in emitted or reflected light. Transmissive measurements deal with light intensities that are 40–60 dB stronger than reflective models, but reflective measurements can be conducted anywhere on the human body, including the thumbs, fingers, or earlobes. Therefore, optical sensing methods are increasingly employed in wearable devices such as wrist-worn fitness trackers for continuous and long-term physiological monitoring. Light transmission varies with wavelength, and IR light bears a relatively broad sensitivity range and resolution for measuring physical alterations in blood vessels. Consequently, an appropriate wavelength range must be selected to enable the transmission capability and resolution required for observing these micro-structural variations.

ECG signals result from ventricular contractions, whereas PPG pulses are generated by vasoconstriction. Each PPG pulse trails an ECG signal, and their combination yields information on pulse transit time and blood velocity. This information can be utilized to formulate a characteristic equation for estimating systolic and diastolic blood pressure and to continually monitor blood pressure [04-05]. It can estimate physiological parameters such as the stiffness index (SI) or reflection index (RI). This optical sensing technique is employed in noninvasive evaluations of arteriosclerosis or cardiovascular disease risk. The advantages and limitations of ECG and PPG measurements are described as follows:

- ECG measurement: Commercial ECG firmware is utilized as a straightforward, first-line measurement tool for the early detection of heart disease. However, ECG signals (mV) are faint and do not surpass a few hundred Hz in frequency, rendering them susceptible to interference from the harmonics of a power source in a 50 Hz or 60 Hz range, which can be eliminated using a band-rejection filter. Consequently, ECG measurements necessitate skin contact, resulting in contact impedance from the skin. Mismatched impedance can result in increased measurement errors (artifacts). Furthermore, it needs to overcome contact noise and electromagnetic interference. In practical application, ECG measurement is a time-consuming method for monitoring in a hospital environment and requires data interpretation by medical staff.
- PPG measurement: Interference with optical measurements stems from noise caused by ambient light, sweat, and motion vibrations. Ambient light, such as from fluorescent bulbs, may contain noise with alternating current components. This interference can be reduced using digital filters. Wearable PPG sensors, when in use during dynamic activities, can generate interferences owing to the relative motion between the optical sensor and the skin, resulting in reduced signal sensitivity. Additionally, the frequency of motion vibrations can be misinterpreted as the RR and must be compensated for when recording measurements during dynamic activities.

Contact measurements require the placement of electrodes or optical sensors on the skin and an external connection to a data processor with signal-conducting wires. Long-term monitoring with this setup can cause discomfort to patients and limit their

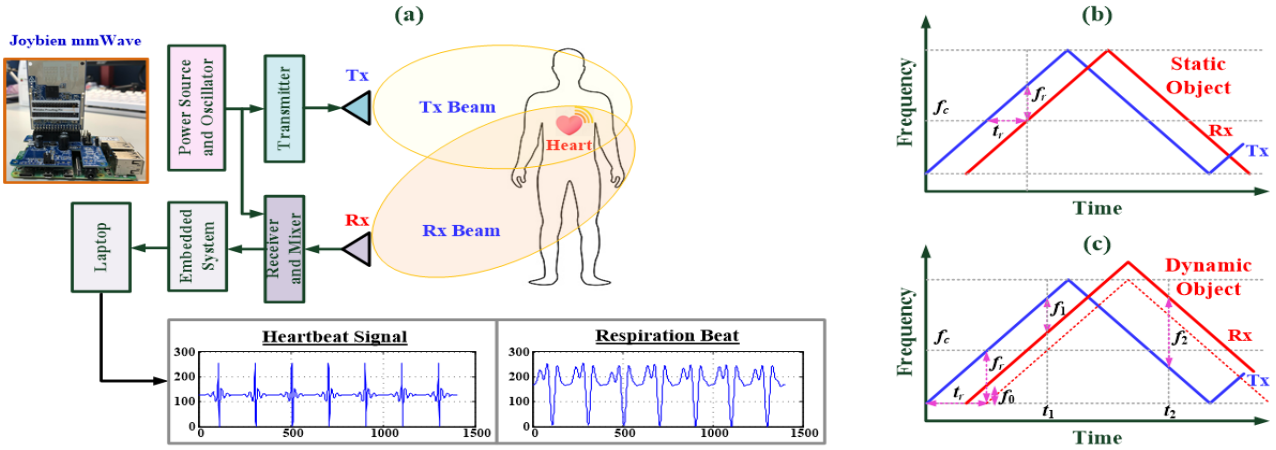

Figure 1. Doppler millimeter (mm)-wave radar-based contactless measurement system. (a) Vital signs (HR and RR detection) continuous monitoring with a mm-wave sensing system; (b) detection of frequency displacements (f_r) produced by a static object; and (c) detection of frequency displacements produced by a dynamic object

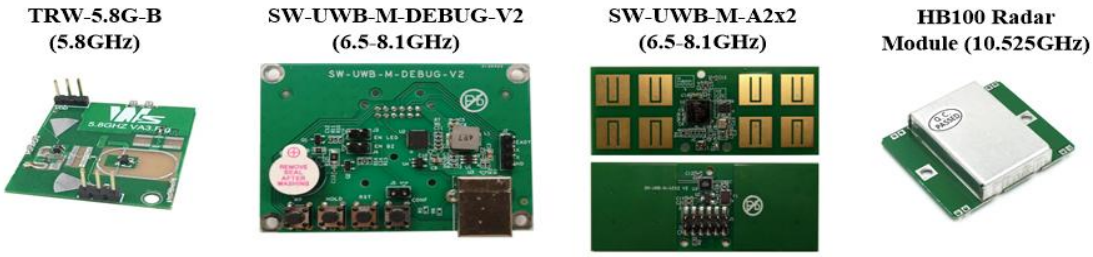

Figure 2. Commercial mm-wave radar circuit boards and embedded modules

movements. Non-contact measurements, on the other hand, do not cause discomfort or adverse biological reactions such as infections, skin irritations, or allergic reactions. Clinically, non-contact measurements are suited to special cases, such as burn patients, as they do not necessitate direct contact with the wound, thus reducing the risk of infection. Given the emergence of new infectious diseases over the past three years, such as SARS, MERS, and COVID-19 [09-10], patients may experience hypoxia, inflicting damage to blood vessels (endothelial dysfunction or arteriosclerosis), the heart, the autonomic nervous system (as indicated by HRV), and systemic inflammatory response or autoimmune disorder. These conditions are especially noticeable in patients with cardiovascular disease. Consequently, the development of non-contact measurement devices is essential to monitor physiological parameters and prevent human-to-human transmission of disease. Additionally, non-contact monitoring bypasses issues such as signal-conducting wires falling off and enables long-term, continuous monitoring.

As depicted in Figure 1(a), this study applies the Doppler effect and frequency-modulated continuous wave (FMCW) radar technology [11] to vital signs detection (VSD), including HR and RR estimation [12–19]. The millimeter (mm)-wave bands of the radar can be segmented into the C-band (4 – 8 GHz), X-band (8 – 12.5 GHz), K-band (12.5 – 40.0 GHz), V-band (40 – 75 GHz), and W-band (75 – 110 GHz). Among these mm-wave bands, the 3 – 30 GHz mm-wave is commonly used in everyday life, with the X-band being a standard range for radar applications in various industries and healthcare. For instance, commercial mm-wave circuit boards (TRW-5.8G-B and HB100 Radar) [14] and embedded modules (SW-UWB-M-DEBUG-V2 and SW-UWB-M-A2x2), as seen in Figure 2, generally operate within specific bands in the 5.8 GHz, 6.5 – 8.1 GHz, or 10.525 GHz ranges. The commercial SW-UWB-M-A2x2 radar module, with a lower transmission frequency, offers a broad detection range of 0.5 – 3.0 m. X-band mm-wave sensors are widely utilized in applications such as theft deterrence, traffic speed detection, automated controls, and VSD. However, owing to its common use, the X-band encounters more significant interferences. The K-band is primarily employed for highly discriminant validity measurements, but because of atmospheric attenuation, its detection range is relatively short, less than 1.0 m [14, 17-18, 20-21].

Therefore, this study employs the Doppler effect and FMCW-based mm-wave sensing method is used to detect human hand tremor [14], pulse wave measurements, RR, and HR [17-21]. In this study, we utilize a W-band mm-wave (76 – 81 GHz) sensing firmware for VSD applications. This is because its radio frequency transmission circuit and microcontroller can integrate into an mm-wave embedded system (utilizing semiconductor processing technology). This system pre-processes sensing signals and then transmits them to a laptop for digital data analysis. Distance and direction can be estimated by analyzing frequency differences between the transmitted and reflected electromagnetic waves, as seen in Figures 1(b) and (c). This can be applied for the detection, tracking, and navigation of dynamic or static objects. We employ the Doppler radar to detect heartbeat and breathing rhythm signals in non-contact measurements and use digital filters to eliminate interferences such as micro-disturbances from the body, background noise, and DC offsets in the system. Additionally, in short-range detection, shorter wavelength radar can bypass the reception of unwanted signals, thereby reducing measurement errors in the intermodulation signals. These unwanted interference components can be mitigated or completely eliminated. Through digital signal processing methods on a laptop, unwanted low-frequency and high-frequency signals can be filtered with a band-pass filter to yield physiological parameters suitable for estimating HR and RR.

In this study, we estimate HR and RR using the frequency-domain and time-domain methods. The frequency-domain method employs the fast Fourier transform (FFT) to extract characteristic frequencies from the post-processing signals. Typically, specific ranges of characteristic frequencies are 1.1 - 1.3 Hz for heartbeat signals and between 0.00 Hz and 0.40 Hz (0.15 – 0.40 Hz) for breathing rhythm signals [22], which is less than 1.0 Hz. HR and RR can both be estimated using these specific characteristic frequencies, with a resting HR of 60 – 70 beats per minute for an adult human and a resting RR of 12 – 20

breaths per minute, both of which gradually increase during exercise. The time-domain method uses the peaks of the heartbeat signal as a benchmark to estimate the average HR with the average R-R interval [04].

We establish a Doppler mm-wave Radar, as depicted in Figure 1(a), which employs non-contact and short-range measurement to capture heartbeat and breathing rhythm signals. This setup enables us to extract characteristic frequencies and parameters to determine HR and RR in both time and frequency domains, respectively. Through experimental tests, we use the results to verify that the data captured by the mm-wave radar can be utilized in real-time human vital signs monitoring, thereby demonstrating the accuracy of mm-wave radars in non-contact measurements.

2. Methodology

2.1. Principles of Contactless mm-Wave Radar Sensing

As seen in Figure 1(a), the non-contact mm-wave radar used in this study is a 71–86 GHz mm-wave sensing firmware device (76–77 GHz: 14 dB; 77–81 GHz: 15 dB). This device consists of a radar mm-wave sensor (Joybien mm-wave IWR 1642 single chip), a Raspberry-Pi Hat Board (ARM Cortex-R4F-based radio control system), and Python application software [11]. Utilizing the Doppler effect, as depicted in Figure 1(a), an electromagnetic wave is emitted from the transmitter end, Tx, toward a static or dynamic object. This object then reflects the electromagnetic wave back to the receiving end, Rx. The digital signal processor captures and processes the reflected signal, facilitating the estimation of the object's motion, distance, speed, and direction or angle based on frequency changes, as depicted in Figure 1(b) and 1(c), respectively. Currently, three dominant mm-wave radar technologies exist: (1) pulse modulation (PM); (2) continuous wave (CW); and (3) frequency modulation (FM) [12–15]. Unmodulated CW radars can detect Doppler frequency shifts caused by changes in object velocity. The object's distance must be measured with FM, whereas PM can only detect the object's distance. The FMCW method can simultaneously detect both an object's distance and velocity [11, 16–18]. In this study, we employ a Doppler radar to perform continuous, non-contact, short-range measurement of human VSD by estimating HR and RR based on frequency differences between the Tx and Rx ends.

Figure 1(b) depicts the incident electromagnetic wave striking a static object [16–18]. The reflected incident wave exhibits identical waveforms and frequencies. A time delay, t_r, develops between both electromagnetic waves due to the distance, d_0; the distance between the object and the radar can be represented as $d_0 = c \cdot t_r / 2$, with c representing the signal propagation velocity in the air and is given as $c = 3 \times 10^8$ m/s. Let the object's motion signal, $x(t)$, as [14]

$$x(t) = A_0 \cos(2\pi f_0 t) \tag{01}$$

where A_0 is the amplitude and f_0 is the frequency. Given f_T and $\theta(t)$ as the transmitted frequency and phase noise, the reflected signal, $R(t)$, can be represented as

$$R(t) \approx A_R \cos(2\pi f_T t) - \frac{4\pi d_0}{\lambda_T} - \frac{4\pi x(t)}{\lambda_T} + \theta(t - \frac{2d_0}{c})) \tag{02}$$

where A_R is the amplitude of the signal $R(t)$; $\lambda_T = c / f_T$ is the wavelength; and d_0 is the fixed distance between the object and the stationary radar sensor. Suppose $\theta_0 = 4\pi d_0 / \lambda_T$ be the phase shift and $\Delta\theta(t) = \theta(t) - \theta(t\text{-}2d_0/c)$ be the residual phase noise, with the mixing process, we can obtain the normalized baseband signal, $B(t)$, as follows [14]

$$B(t) \approx \cos(\theta_0 + \frac{4\pi x(t)}{\lambda_T} + \Delta\theta(t)) \tag{03}$$

Considering θ_0 as an odd multiple of $\pi/2$ and $x(t) << \lambda_T$, we can simplify the equation (03) as

$$B(t) \approx \frac{4\pi x(t)}{\lambda_T} + \Delta\theta(t) \tag{04}$$

Figure 1(c) shows that if the object is in motion, the electromagnetic wave is reflected by a target moving relative to the radar, and then the reflected electromagnetic wave demonstrates a frequency shift f_d; the frequency changes of processed signal can be expressed as "$f_1 = f_r - f_d$" and "$f_2 = f_r + f_D$", respectively. The distance between the radar and the object can be estimated as $D = (c / (4 \times f_m \times b)) \times ((f_2 + f_1)/2)$, where f_m indicates the modulation frequency, and b represents the maximum change in the modulation frequency. The relative velocity of the dynamic object is $v = (c / (2 \times f_c)) \times ((f_2 - f_1)/2)$, where f_c denotes the center frequency of the incident electromagnetic wave [16–18], enabling the detection of the dynamic object's distance and motion velocity.

Table 1. Specifications of the Doppler mm-wave radar [11]

Hardware	Specification
FMCW based Transceiver	• 76- 81GHz Coverage With 4 GHz Continuous Bandwidth; • Four Receive Channels; • Two Transmit Channels; • Ultra-Accurate Chirp (Timing) Engine Based on Fractional-N PLL • Rx Noise Figure: 14 dB (76 to 77 GHz) / 15 dB (77 to 81 GHz)
DSP (Digital Signal Processor)	C674x DSP for FMCW Signal Processing
MCU (Micro Controller Unit)	• ARM Cortex-R4F Microcontroller for Application Control • I/O: SPI / CAN × 1 • Up to 2 UARTs I2C × 1 (Raspberry Pi Hat Board (ARM® Cortex® -R4F-Based Radio Control System)
Intend Purpose	Vital Signs Detection (VSD) Firmware for Short-Distance (30 - 90cm Wireless and Contactless Detection for Heart Rate (HR) and Respiration Rate (RR) ONLY one of VSD; HAM (Pre-programmed within a Single mmWave Module)
Operating Temperature and Humidity	• 0° to 40° degree Celsius • 10% - 85% Non-Condensing

After receiving the processed signal, the measurement data are routed to a data acquisition system through a serial communication line for analog-to-digital conversion (ADC) and digital signal processing. Thus, $x(t)$ in equation (04) can be expressed as follows [19]:

$$x(t) \approx x_h(t) + x_b(t) + \Delta d(t) \tag{05}$$

where $x_h(t)$ and $x_b(t)$ represent the distance variation caused by heartbeat and breathing rhythms, and $\Delta d(t)$ denotes the residual signal. For the short-range measurement (< 1.0 m), the residual phase noise, $\Delta\theta(t)$, and the residual signal, $\Delta d(t)$, can be neglected [19]. In digital signal processing, a digital filter, or band-pass filter, is employed to sift out unwanted high- and low-frequency components. This way, we can isolate the heartbeat and breathing rhythm signals, $x_h(t)$ and $x_b(t)$. Subsequently, FFT can be used to estimate the characteristic frequencies of signals, $x_h(t)$ and $x_b(t)$ [23, 24]. Table 1 presents the specifications of the non-contact and short-range mm-wave sensor used in this study [11]. The proposed mm-wave radar eschews the need for contact sensors or signal-conducting wires and can continuously monitor human vital signs in real-time. This renders it especially useful for patients with severe infectious diseases (e.g., SARS, MERS, and COVID-19), serious and acute respiratory disorders, or burns.

2.2. HR and RR Estimations

Human heartbeats and breathing rhythms are not fixed and are primarily regulated by the human autonomic nervous system. These heartbeats and breathing rhythms can be analyzed using frequency-domain and time-domain methods to determine HR and RR. In both methods, fragmented rhythm signals (approximately 10 rhythm signals, as observed in Figures 3(a) and 4(a)) are used to

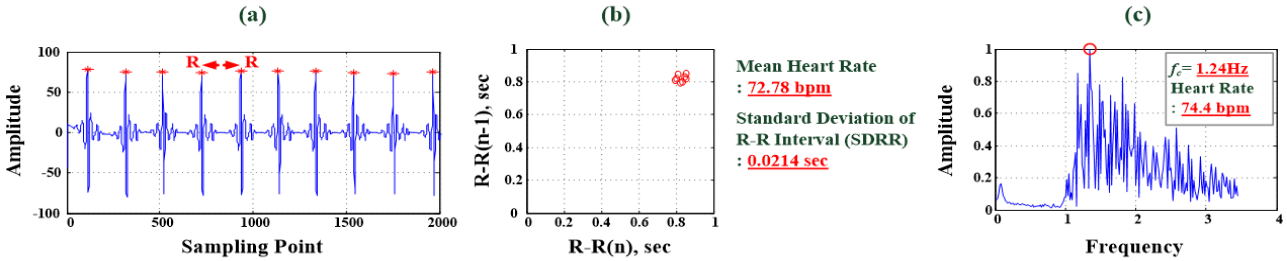

Figure 3. Time-domain and frequency-domain analysis for heartbeat signals. (a) Time-domain raw data for heartbeat signals, (b) Time-domain R-R interval analysis (HR = 72.78 bpm), and (c) frequency-domain HR analysis (f_{c1} = 1.24 Hz, HR = 74.4 bpm)

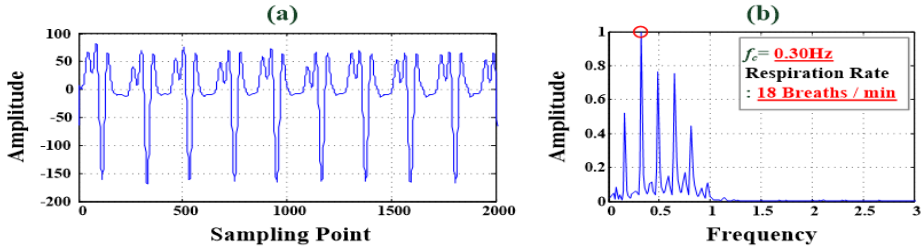

Figure 4. Time-domain and frequency-domain RR analysis for breathing rhythm signals. (a) Time-domain raw data for breathing rhythm signals, (b) Frequency-domain analysis for RR estimation (f_{c2} = 0.30 Hz, RR = 18 breaths/min)

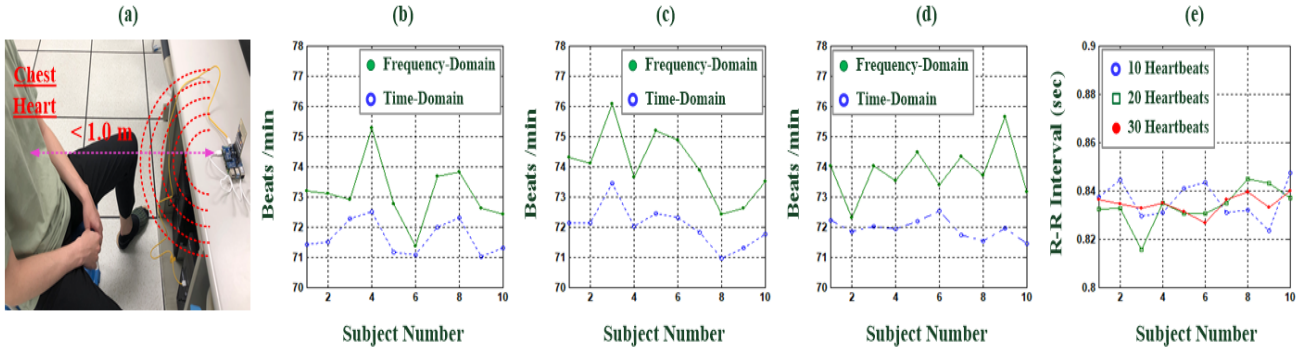

Figure 5. Experimental setup and frequency- and time-domain analysis for HR estimation. (a) Experimental setup for VSD tests, (b) Frequency- and time-domain analysis for HR estimations with 10 heartbeats, (c) HR estimations with 20 heartbeats, (d) HR estimations with 30 heartbeats, (e) R-R interval estimations with 10, 20, and 30 heartbeats

estimate the HR and RR, respectively. In frequency-domain analysis, rhythm signals are transformed into a spectrogram using the FFT method to identify the characteristic frequencies, as seen in Figures 3(c) and 4(b), respectively. The HR and RR can be estimated by using the following equations:

- HR = 60 × f_{c1} (beats / min) (06)
- RR = 60 × f_{c2} (breaths / min) (07)

Here, f_{c1} represents the characteristic frequency of the fragmented heartbeat signals, and f_{c2} denotes the characteristic frequency of the fragmented breathing rhythm signals, respectively. For adults, the main frequency ranges within 1.1 – 1.3 Hz for heartbeat, and the main frequency for breathing rhythm signals ranges between 0.15 and 0.40 Hz. Lower frequency ranges, 0.04 – 0.15 Hz, reflect regulatory responses by the sympathetic and the parasympathetic systems.

In time-domain analysis, the R peak detection in each heartbeat signal is the basis, as seen in Figure 3(a). Each R-R interval can be estimated between the R peak and the subsequent one, as displayed in Figure 3(b). The average R-R interval, denoted as $R\text{-}R_{ave}$, provides the mean HR, as demonstrated in Equations (08) and (09).

$$R\text{-}R_{ave} = \frac{1}{M}\sum_{m=1}^{M} R\text{-}R_m \text{ (sec)} \quad (08)$$

$$HR = \frac{60}{R\text{-}R_{ave}} \text{ (beats / min)} \quad (09)$$

Thus, Equations (06)–(09) can be employed to estimate physiological parameters and indicators in real-time. Normal r anges for adults are 48 < HR < 120 (beats / min) and 6 < RR < 30 (breaths / min), with slight variations based on factors such as age, sex, body weight, and health. These indices can assist in the early detection of life-threatening symptoms, such as coughing and shortness of breath, which are indicative of respiratory issues such as chronic obstructive pulmonary disease or acute respiratory distress syndrome (ARDS).

3. Experimental Results and and Discussions

3.1. Experimental Setup

Experiments, tests, and validation of human VSD were conducted using the contactless sensor based on mm-wave radar depicted in Figure 1(a). The experimental setup employed a Doppler radar mm-wave sensing system [11], which included a 76 – 81GHz (W-band) Doppler radar millimeter-wave sensing firmware (Joybien mm-Wave) with a Tx electromagnetic wave transmitter and an Rx electromagnetic wave receiver, a Raspberry-Pi Hat Board (ARM Cortex-R4F), an ADC, a microcontroller unit, and a digital signal processor. This sensing system, utilizing the FMCW method, is designed for VSD over a short-range of 0.3 – 0.90 m. This system can link to the internet of medical things (IOMT) systems via built-in Wi-Fi or Bluetooth wireless communication [25] for transmitting physiological measurements. This can be achieved through 2.4 – 2.485 GHz or 5.0 – 6.0 GHz ISM (Industrial, Science, and medical, excluding applications in telecommunications) radio bands standard (IEEE 802.11 Wireless Networking Protocol [27]). The 5G (fifth-generation) communication system [26] facilitates the transmission of a

Table 2. Comparison of millimeter-wave radar, ECG, and PPG detection.

VSD Methods	Millimeter (Mm)-wave Radar	ECG Measurement	PPG Measurement
Principles (Technology)	Doppler radar detection of millimeter waves	Detection of physiological signals from the heart through electrodes on the skin	Optical detection of pulse signals through direct contact with the skin
Detection Signals	76–81 GHz electromagnetic waves (incident and reflected electromagnetic waves)	Heart nerve conduction signals (changes in cardiomyocyte depolarization voltages)	Infrared light (650 nm) or near-infrared light (800–940 nm)
Detection Approach	Contactless Sensing	Contact Sensing	Contactless / Contact Sensing
Detection Distance	Short-range (30–90 cm)	Active or passive detection through electrodes on skin	Transmissive and reflective light sensors on the skin
Wearable ?	×	√	√
Sources of Interference and Noise	Uses short-wavelength mm-wave and short-range measurement to avoid unnecessary environmental noise (slight)	Power harmonic interference (50 Hz/60 Hz), skin contact impedance interference, electromagnetic interference, interference caused by human vibrations	Interference from ambient light (fluorescent lights and energy-saving lamps), sweat, and motion vibrations
Filter Requirement ?	√	√	√
Monitoring Type	Continuous monitoring	Continuous monitoring	Continuous monitoring
Movement Restrictions?	×	√	√
Medical Purpose (Applications)	HR and RR Estimation	• HR and RR Estimation • Sympathetic nerve activity evaluation • Temperature regulation response evaluation • Peripheral cardiovascular tone and reflex evaluation	• HR and RR Estimation • SPO_2 Estimation • Blood Flow Velocity Estimation • Stiffness Index (SI) Estimation • Reflection Index (RI) Estimation

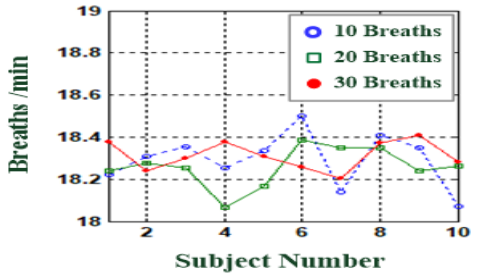

Figure 6. Frequency-domain analysis for RR estimations with 10, 20, and 30 breaths

patient's data to remote hospitals or a clinician's smart phone and iPad, enabling hospitals, patients, and their families to monitor physiological parameters. This information can then be used in multiparty consultations and patient discussions. The Raspberry-Pi Hat Board provides an integrated development environment, namely "Geany", for writing Python application programs. These programs are used to implement the mm-wave FMCW control, FFT operation, and time-domain analyses for processing the raw data and deriving the real-time HR and RR estimations.

3.2. Experimental Tests and Discussion

The contactless VSD experiments and tests for short-range (< 1.0 m) were conducted in a laboratory, as portrayed in Figure 5(a). Participants were young adult males with an average age of 22 years. Each participant underwent a static VSD test, recording heartbeats and breathing data for a one-minute interval for each test. For instance, fragmented raw data from 10 instances of heartbeats and breathing rhythms are portrayed in Figures 3(a) and 4(a), respectively. Using time-domain analysis to determine the R-R interval, Equations (08) and (09) were employed to calculate the mean HR. As demonstrated in Figure 3(b), the mean HR for the 10 heartbeats depicted in Figure 3(a) is 72.7800 bpm. Results from the frequency-domain analysis are displayed in Figure 3(c) and Figure 4(b), extracting the main characteristic frequencies, f_{c1} = 1.24 Hz and f_{c2} = 0.30 Hz, for 10 instances of heartbeats and breathing rhythms. Equations (06) and (07) reveal that HR = 74.4 beats/min and RR = 18 breaths/min, respectively.

Figures 5(b), 5(c), and 5(d) present HRs based on 10, 20, and 30 heartbeats, respectively, during static human VSD. The time-domain analysis resulted in average HRs of 71.66, 72.03, and 71.94 beats/min, and average R-R intervals of 0.8361 s, 0.8336 s, and 0.8345 s. Figure 5(e) illustrates that the time-domain analysis yielded average HRs of 73.11, 74.06, and 73.68 beats/min. All participants were healthy young men, with their average HRs falling within the normal range of 48 < HR < 120 (beats/min). Figure 6 presents frequency-domain RR analysis based on 10, 20, and 30 breaths; the average RRs were observed to be 18.29, 18.26, and 18.31 breaths/min, respectively. These results are within the normal RR range of 6 < RR < 30 (breaths/min). Subsequently, the experimental results from the 10 participants for a 1 minute static VSD test were utilized to validate the feasibility of the mm-wave radar sensing system constructed in this study, which could perform contactless and short-range measurements for HR and RR estimations. A comparison of the mm-wave radar to ECG and PPG detection methods is presented in Table 2.

ECG measurement captures a weak voltage signal through active or passive electrodes on the skin. The sensing circuit requires a high-gain and high-pass filter (cutoff frequency: 0.3 Hz) along with a low-pass filter (cutoff frequency: 37.0 Hz), and a signal gain of about 100, which can filter out additional high- and low-frequency noises. This contact sensing circuit can readily be integrated into a wearable device. Clinically, 12 leads can be used to measure ECG signals from limb and chest leads, but continuous monitoring of cardiac electrical activity signals can be hampered by the numerous signal conducted wires which restrict patient movement and affect measurement quality. PPG measurement uses single or dual-wavelength light sources to measure pulse signals and oxygen saturation in transmissive or reflective modes. Although reflective mode can be used on any part of the body, the signal must undergo further processing such as noise filtering, signal amplification, signal modulation, and signal digitization when the optical detector receives light flux changes. Optical detectors are compact and lightweight, with photoemitters, photoreceivers, and driver circuits easily integrated into embedded systems. Current commercial optical detector IC firmware can suppress ambient light, reduce power consumption, and extend monitoring time.

ECG and PPG measurements can be utilized to detect peripheral arterial disease (PAD) by assessing a patient's arteriosclerosis risk level [03, 28] Specific pulse characteristic parameters can be derived and analyzed from the time-domain PPG waveforms, such as the time intervals between pulse waves and the peak height ratios of the pulse signals, to estimate the

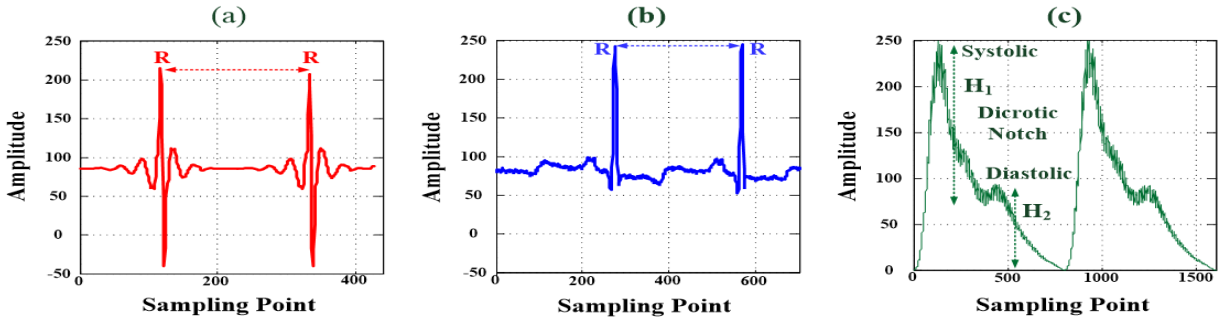

Figure 7. ECG and PPG signals of vital signs: (a) millimeter-wave radar detection of ECG signals; (b) lead II detection of ECG signals; and (c) infrared photoreceiver detection of PPG signals

SI (Stiffness Index) and RI (Reflection Index) indexes. For instance, RI = (H_2 / H_1) × 100%, as seen in Figure 7(c). The 76 – 81 GHz mm-wave radar developed in this study offers several advantages compared to ECG and PPG measurements:

- It enables contactless and short-range sensing.
- It offers suitable directionality from the mm-wave antenna emitting electromagnetic waves, which aids in controlling the sensing range.
- It bears a strong resistance to interference from environmental factors such as temperature, humidity, noise, airflow, dust, and light.
- It exhibits a high level of resistance to radio frequency interference.
- It produces low output power that is harmless to humans.

Figures 7(a) and (b) depict the raw data from the mm-wave radar and a lead II ECG, respectively. Both time-domain waveforms exhibit periodic R peaks, which are used to estimate the R-R interval. From these, the average HR can be calculated using Equations (08) and (09). In this study, the 76 – 81 GHz mm-wave radar sensing firmware demonstrated the capability for contactless and short-range detection of heartbeat signals. Numerous ECG and PPG measurements were gathered and tested. In addition to VSD, these data can be used to evaluate peripheral arterial disease, cardiac arrhythmia, arteriosclerosis, sympathetic nervous activity, and temperature regulation responses. ECG has been used to detect arrhythmia types, heart conduction abnormalities, coronary ischemia, and atrial fibrillation based on the detected P wave, QRS complex wave, and T wave. Future research should aim to acquire extensive amounts of ECG signals from patients with cardiac arrhythmia to verify the applicability of the 76–81 GHz mm-wave radar for detecting cardiac arrhythmia.

4. Conclusion

IOMT systems enable the collection and exchange of measurement data between the user-end and the sensor-end. This can be actualized through the continuous collection of heartbeat and breathing signals, blood pressure, and other biochemical examination data. Physiological signals captured *via* VSD can be analyzed based on their frequency-domain and time-domain characteristic parameters to assist in detecting early symptoms of cardiopulmonary diseases. Contactless and short-range VSD was conducted on a group of healthy young men using a 76 – 81 GHz mm-wave radar within a 30–90 cm range. The promising HR and RR results obtained with this mm-wave radar device validate its feasibility for contactless detection.

During the COVID-19 pandemic, which has caused persistently high disease levels worldwide over the past three years (2019 – 2023 years), VSD became a necessity in the quarantine and treatment of confirmed cases owing to concerns about human-to-human transmission and other infectious disease control issues. Future instrument designs must incorporate contactless, short-range detection, and online collaboration features. The 76 – 81 GHz mm-wave radar can assist with continuous vital sign monitoring, and integration with the internet and 5G communication technologies can facilitate the processing of the massive volume of data collected in IOMT systems. Moreover, this integration can enable data analysis and AI applications on user-end devices, such as machine learning (ML) and deep learning (DL) based diagnostic tools.

The feasibility of the mm-wave radar in this study for contactless VSD has been verified, and this device may be applied in future clinical practices to monitor heartbeat signals related to atrial fibrillation, supraventricular tachycardia, ventricular tachycardia, and heart block. The further development of ML or DL based classifiers may enable the identification of different arrhythmia types. Consequently, the mm-wave radar with an AI-based classifier will be considered a Class II medical device, and its development requires evaluations of electrical safety, effectiveness, accuracy, and device risk (IEC60601 [29]), as well as clinical testing before integration into IOMT systems.

Acknowledgment

This work was supported by the **National Science and Technology Council (NSTC)**, under contract number: **NSTC 111-2221-E-167- 034**, duration: August 1, 2022 – July 31, 2023; and also supported by the National Chin-Yi University of Technology, under contract number: **NCUT 23-R-CE-009**, duration: January 1, 2023–November 30, 2023.

References

[01] John Allen, “Photoplethysmography and its application in clinical physiological measurement, ”Physiol. Meas., vol. 28, no. 3, 2007, pp. R1-39.

[02] Panicos Kyriacou and John Allen, Photoplethysmographyechnology, Signal Analysis and Applications, 1st Edition, 2021, ISBN 9780128233740.

[03] Jian-Xing Wu, Chia-Hung Lin, Chung-Dann Kan, and Wei-Ling Chen, “Bilateral photoplethysmography for peripheral arterial disease screening in hemodialysis patients using astable multivibrator and machine learning classifier, ”IET Science, Measurement & Technology, vol. 13, no. 9, 2019, pp. 1277- 1286.

[04] Chia-Hung Lin, Jian-Xing Wu, Pi-Yun Chen, Chien-Ming Li, Neng-Sheng Pai, and Chao-Lin Kuo, “Symmetric cryptography with a chaotic map and a multilayer machine learning network for physiological signal infosecurity: case study in electrocardiogram, ”IEEE Access, vol. 9, 2021, pp. 26451- 26467.

[05] Chia-Hung Lin, Jian-Xing Wu, Neng-Sheng Pai, Pi-Yun Chen, Chien-Ming Li, and Ching Chou Pai, “Intelligent physiological signal infosecurity: case study in photoplethysmography (PPG) signal, ”IET Signal Processing , vol. 16, no. 3, 2022, pp. 267- 280.

[06] Md Rizman Md Lazin Md Lazim, Amilia Aminuddin, Kalaivani Chellappan, Azizah Ugusman, Adila A Hamid, Wan Amir Nizam Wan Ahmad, and Mohd Shawal Faizal Mohamad, “Is heart rate a confounding factor for photoplethysmography markers? A systematic review, ”International Journal of Environmental Research and Public Health, vol. 17, 2020, pp. 1-12.

[07] John Allen, Klaus Overbeck, Alexander F. Nath, Alan Murray, and Gerard Stansby, “A prospective comparison of bilateral photoplethysmography versus the ankle-brachial pressure index for detecting and quantifying lower limb peripheral arterial disease, ”Journal of Vascular Surgery, vol. 47, no. 4, 2008, pp. 794-

802.
[08] Emma J Sharkey, Costanzo Di Maria, Annette Klinge, Alan Murray, Dingchang Zheng, John O'Sullivan, and John Allen, “Innovative multi-site photoplethysmography measurement and analysis demonstrating increased arterial stiffness in paediatric heart transplant recipients, ”Physiological Measurement, vol. 39, no. 7, 2018, pp. 074007.
[09] Han Jin, Shengwen Yang, Fan Yang, Long Zhang, Haoyu Weng, Shengcong Liu, Fangfang Fan, Haichao Li, Xizi Zheng, Hongyu Yang, Yan Zhang, Jing Zhou, and Jianping Li, “Elevated resting heart rates are a risk factor for mortality among patients with coronavirus disease 2019 in Wuhan, China,”J Transl Int Med., vol. 9, no. 4, 2021, pp. 285–293.
[10] Araújo Cláudia Regina da Silva, Fernandes Juliana, Caetano Débora Sidrônio, Barros Ana Eugênia Vasconcelos do Rêgo, de Souza Juliana Andrade Ferreira, Machado Maria da Glória Rodrigues, de Aguiar, Maria Inês Remígio, Brandão Simone Cristina Soares, Campos Shirley Lima, de Andrade Armele de Fatima Dornelas, and Brandão Daniella Cunha, “Endothelial function, arterial stiffness and heart rate variability of patients with cardiovascular diseases hospitalized due to COVID-19, ”Heart Lung, vol. 58, 2023, pp. 210-216.
[11] Joybien Technologies Co,. Ltd., Joybien mmWave, 2023 years, available: https://computer-consultant-1700.business.site/ and http://www.joybien.com/.
[12] B. Dekker, S. Jacobs, A. S. Kossen, M. C. Kruithof, A. G. Huizing, and M. Geurts, “Gesture recognition with a low power FMCW radar and a deep convolutional neural network, ”2017 European Radar Conference, Nuremberg, Germany, 2017.
[13] Bo Peng, Zhen Liu, Xizhang Wei, and Xiang Li, “Sinusoidal frequency modulation sparse recovery for precession rate estimation using low-frequency long-range radar, ”IEEE Sensors Journal, vol. 15, no. 12, 2015, pp. 7329-7340.
[14] Chia-Hung Lin, Jian-Xing Wu, Jin-Chyr Hsu, Pi-Yun Chen, Neng-Sheng Pai, and Hsiang-Yueh Lai, “Tremor class scaling for parkinson disease patients using an array X-band microwave Doppler based upper limb movement quantizer, ”IEEE Sensors Journal, vol. 21, no. 19, 2021, pp. 21473-21485.
[15] IEEE Aerospace and Electronic Systems Society, IEEE Standard 686-2017 for radar definitions, IEEE Std 686-2017, 2017.
[16] Daeun Jung, Sungpil Cheon, Dongryul Kim, JoonseokYoon and Byungkwan Kim, “Short time remote heart rate measurement based on mmWave FMCW radar frame structure, ”IEEE Antennas and Wireless Propagation Letters (Early Access Atricle in Press), vo. 14, no. 8, 2021, pp. 1-5.
[17] Zongquan, Ling, Weinan Zhou, Yuhao Ren, Jiping Wang, and Liquan Guo, “Non-contact heart rate monitoring based on millimeter wave radar, ”IEEE Access, vol. 2022, pp. 74033-74044.
[18] Fengyu Wang, Xiaolu Zeng, Chenshu Wu, Beibei Wang, and K. J. Ray Liu, “Driver vital signs monitoring using millimeter wave radio, ”IEEE Internet of Things Journal, vol. 9, no. 13, 2022, pp. 11283-11298.
[19] Fengyu Wang, Feng Zhang, Chenshu Wu, Beibei Wang, and K. J. Ray Liu, “ViMo: Multiperson Vital Sign Monitoring Using Commodity Millimeter-Wave Radio, ”IEEE Internet of Things Journal, vol. 8, no. 3, 2021, pp. 1294-1307.
[20] Ghufran Shafiq and Kalyana C. Veluvolu, “Surface chest motion decomposition for cardiovascular monitoring, ”Scientific Reports, vol. 4, 2014, pp. 1-9.
[21] Kuo-Kai Shyu, Luan-Jiau Chiu , Po-Lei Lee, and Lung-Hao Lee, “UWB simultaneous breathing and heart rate detections in driving scenario using multi-feature alignment two-layer EEMD method, ”IEEE Sensors Journal, vol. 20, no. 17, 2020, pp. 10251-10266.
[22] S. Akselrod, D. Gordon, F. A. Ubel, D. C. Shannon, A. C. Berger, and R. J. Cohen, “Power spectrum analysis of heart rate fluctuation: a quantitative probe of beat-to-beat cardiovascular control, ” Science, vol. 213, no. 4504, 1981, pp. 220-222.
[23] Ainara Garde, Walter Karlen, Parastoo Dehkordi, Jm Ansermino, and G.. Dumont, “Empirical mode decomposition for respiratory and heart rate estimation from the photoplethysmogram, ” Computing in Cardiology, vol. 40, 2013, pp. 799- 782.
[24] B. Prathyusha, T. S. Rao, and D. Asha, “Extraction of respiratory rate from PPG signals using PCA and EMD, ” International Journal of Research in Engineering and Technology, vol. 1, no. 2, pp. 164-184, 2012.
[25] Ali Ghubaish, Tara Salman, Maede Zolanvari, Devrim Unal, Abdulla Al-Ali, and Raj Jain, “Recent advances in the internet- of-medical-things (IoMT) systems security, ”IEEE Internet of Things Journal, vol. 8, no. 11, 2021, pp. 8707 –8718.
[26] M. M. Kamal, S. Yang, S. H. Kiani, M. R. Anjum, M. Alibakhshikenari, Z. A. Arain, A. A. Jamali, A. Lalbakhsh, and E. Limiti, “Donut-shaped mmwave printed antenna array for 5G technology, ”Electronics, vol. 10, no. 12, 2021, pp. 1-10.
[27] The Working Group for WLAN Standards, IEEE 802.11™ wireless local area networks, 2023 years, available: https://www.ieee802.org/11/
[28] Jian-Xing Wu, Chien-Ming Li, Yueh-Ren Ho, Ming-Jui Wu, Ping-Tzan Huang and Chia-Hung Lin, “Bilateral photoplethysmography analysis for peripheral arterial stenosis screening with a fractional-order integrator and info-gap decision-making, ”IEEE Sensor Journal, vol. 16, no. 8, April 2016, pp. 2691-2700.
[29] IEC 60601-1:2023 SER Series, Medical electrical equipment, 2023 years, available: https://webstore.iec.ch/publication/2603.